

PRELIMINARY RESULTS ON POTENTIAL DEFORMATIONS OCCURRING ON SLOPES OF MAJOR HIGHWAYS BY ANALYZING SENTINEL 1 IMAGES

Elissavet Chatzicharalampous¹, Constantinos Loupasakis², Issaak Parcharidis³, Manolis Charalampakis⁴, Michaela-Maria Karathanou-Nicholaidi⁵

¹ PhD Student, School of Mining and Metallurgical Engineering, National Technical University of Athens, 9, Ir. Polytechniou str., 15780, Polytechniupoli, Zografou, Athens, Greece, (chatzieliza@central.ntua.gr)

² Associate Professor, School of Mining and Metallurgical Engineering, National Technical University of Athens, 9, Ir. Polytechniou str., 15780, Polytechniupoli, Zografou, Athens, Greece, (cloupasakis@metal.ntua.gr)

³ Professor, Department of Geography, Harokopio University, office 4.3a new bld, 70El. Venizelou str., 17671, Kallithea, Athens, Greece, (parchar@hua.gr)

⁴ Civil Engineer, Egnatia Odos S.A., Thessaloniki, Greece, (mharala@egnatia.gr)

⁵ MSc Student, School of Mining and Metallurgical Engineering, National Technical University of Athens, 9, Ir. Polytechniou str., 15780, Polytechniupoli, Zografou, Athens, Greece, (nicholaidi_micha@hotmail.com)

Key words: *Deformations, Highways, Slopes, Sentinel 1, Multitemporal SAR Interferometry*

ABSTRACT

The use of satellite data and remote sensing methods is a common practice in order to monitor and study instability phenomena, the occurrence of which have large social and economic cost, especially when they affect inhabited areas and major infrastructure. Here after, preliminary results of applying a Multitemporal SAR Interferometry methodology using Copernicus Sentinel 1 scenes, in order to study sections of a Highway in Greece are presented. Specifically, by the use of Gamma Remote Sensing software, ascending and descending Sentinel 1A satellite images have been processed, covering the period from January 2016 to August 2017 (P1), as well as Sentinel 1A and Sentinel 1B ascending and descending acquisitions covering the period from January 2018 to April 2018 (P2). Subsequently, total component (Vol) was calculated for both time periods under study, by taking into account ascending and descending results, for slopes for which E-W component is prevalent. Besides detecting deformation phenomena, purpose of the current study was to examine the effect of the time interval between successive images, in terms of results quality and coverage.

I. INTRODUCTION - AREAS OF STUDY

Last decades, there is a growing evolution in using satellite images and remote sensing methods in different aspects of everyday life and scientific research. One major research field is the detection, mapping and monitoring of land deformation induced by natural or anthropogenic causes (Pecoraro *et al.*, 2019; Frodella *et al.*, 2018; Mazzanti *et al.*, 2017; Gaprindashvili *et al.*, 2016; Cardellini *et al.*, 2015; Roberts *et al.*, 2014; Bernardi *et al.*, 2013; Cardellini *et al.*, 2013).

Land deformation appearing as landslide, land subsidence, etc., may take place in isolated areas without any direct effect to humans and human activity. But when these phenomena affect inhabited areas, infrastructure or areas under exploitation, the impact may be significant, affecting the society, the economy, the transportation and etc. That is the reason why it is of great importance to be able to detect, map and monitor the continuity of these phenomena.

Worldwide, a lot of research has been made focusing on methodologies and algorithms for processing satellite data and methods to apply them for detection, mapping and monitoring of land

deformation, especially landslides, which are considered to be as one of the most damaging form of land deformation (Refice *et al.*, 2019; Yao *et al.*, 2019; Dong *et al.*, 2018; Tessari *et al.*, 2017; Barra *et al.*, 2016; Notti *et al.*, 2015a; Notti *et al.*, 2015b; Plank *et al.*, 2015; Bellotti *et al.*, 2014).

Permanent or Persistent Scatterers Interferometry Synthetic Aperture Radar (PSInSAR) (Ferretti *et al.*, 2000; Ferretti *et al.*, 2001) is the main multitemporal SAR Interferometry technique in order to monitor deformation for long periods and even of millimeter rate. In addition, a lot of other techniques have been developed, based in exploiting either Permanent coherent Persistent Scatterers (PSs) or Temporally coherent Distributed Scatterers (DSs). Small BAseline Subset (SBAS) technique (Bernardino *et al.*, 2002), a Distributed Scatterers method, Interferometric Point Target Analysis (IPTA) (Werner *et al.*, 2003), a Persistent Scatterers technique, are some of these algorithms used for multitemporal SAR Interferometry. Every methodology has advantages and disadvantages and not all methodologies can be applied in all cases, depending on the characteristics of the area under study and data availability. PSs techniques that are based in artificial objects (PSs) that reflect radar

energy well, provide with estimation of velocity for each PS along the Line Of Sight (LOS) of the satellite (Ferretti *et al.*, 2000; Ferretti *et al.* 2001). Terrain deformation maps can be developed by combining many of these measurements. In the case of DSs techniques, the objects (DSs) reflect lower radar energy, in comparison with PSs, usually covering several pixels of the SAR images and therefore can be located even in rural areas. These pixels exhibit similar scattering properties and together are used for estimating deformation. One of the techniques using DSs for developing deformation maps is SBAS.

Typically, for a PSI analysis, a significant number of SAR scenes over the same area is required. In case of smaller stacks, a hybrid methodology was developed where starting from a multireference stack and by the use of an SVD step, single reference time series are derived (Werner *et al.*, 2008).

The areas under investigation in the current paper are sections of Egnatia Highway. Egnatia Highway or else A2 motorway, is part of the E90 European road and the largest motorway of Greece, with a length of 657,50km. Starting from Igoumenitsa in the west, it ends up in Kipouf in Evros in the east. Egnatia is crossing all of northern Greece, mainly through mountainous areas. Its construction begun in 1994 and in total was completed in 2014. From the early stages of designing and constructing of Egnatia Highway, it was clear, to all parts involved, the size of the challenge they had to face, as Egnatia had to cross through areas with intense relief, high altitudes, high inclination and more importantly, through areas with extremely complicated geology and with already known instability phenomena. In most cases it was impossible to change the route of the highway in order to avoid these complicated conditions.

The current study aims to identify potential deformations influencing the operation of the Highway, by processing and analyzing Sentinel 1A and Sentinel 1B images following Multitemporal SAR Interferometry.

Specifically, the research was focused on two sections of Egnatia Highway, passing by the villages of 1) Asomata and 2) Lefkopetra (figure 1).

In these sections the route crosses tunnels, embankments and trenches and they were selected due to the fact that during the construction deformation phenomena related to landslide movements were recorded and stabilization measures had been applied.

Mainly by taking into consideration that the areas under investigation have mountainous topography and are mostly covered by trees, thus with lack of scatterers, a Multitemporal SAR Interferometry was applied. More particularly, a hybrid SBAS type methodology that uses Singular Value Decomposition (SVD) algorithm, in order to obtain the least-squares solution for the phase time-series was applied. With this technique, starting from a multi-reference stack of

unwrapped phases, a single reference time series can be derived by the use of SVD (Wegmüller *et al.*, 2016b).

In this preliminary phase, two separate time periods are examined, one short period (P2) where time interval between successive images is 6 days and a longer one (P1) where time interval is approximately 30 days. Besides detecting the existence of instability phenomena, the purpose of that is to examine the significance of time interval between successive images, in terms of results quality and coverage, for our areas.

On one hand the study proves that the retaining measures applied for the stabilization of the highway provide the necessary safety as we were not able to identify any areas affected by deformation phenomena in progress. On the other hand, it seems that in terms of coverage the results are more detailed in the case of 6 days period time interval.

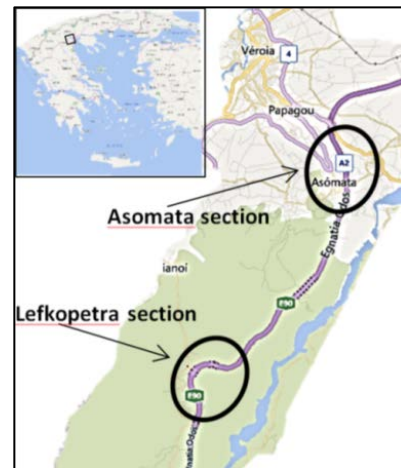


Figure 1. The sections under investigation along the Egnatia Highway (picture not in scale).

II. DATA USED AND ANALYSIS METHODS

Research is based in analyzing Sentinel 1 right-looking satellite images of Ascending, Path 175, and Descending, Path 80, pass, by the use of Multitemporal SAR Interferometry. The scenes obtained and processed are SAR Standard L1 Products of Single Look Complex (SLC) images, Interferometric Wide (IW) swath mode and VV polarization. Two different time periods are analyzed, presenting different time interval between successive images as well. Those are:

- The time period (P1) from January 2016 to August 2017, with time interval between successive images of approximately 30 days,
- The time period (P2) from January 2018 to April 2018, with time interval between successive images of 6 days.

For the time period P1, 45 Sentinel 1A satellite images were analyzed, 22 Ascending and 23 Descending (table 1). For the time period P2, 40 Sentinel 1A and 1B satellite images were analyzed, 20 Ascending and 20 Descending (table 2).

Table 1. List of Sentinel 1A scenes analysed of Ascending (P1A) and Descending (P1D) acquisition geometry, for the time period extending from January 2016 to August 2017

No.	Date	P1A	P1D
1	22 January 2016		P1D
2	28 January 2016	P1A	
3	21 February 2016	P1A	
4	27 February 2016		P1D
5	10 March 2016		P1D
6	16 March 2016	P1A	
7	03 April 2016		P1D
8	09 April 2016	P1A	
9	27 April 2016		P1D
10	03 May 2016	P1A	
11	21 May 2016		P1D
12	27 May 2016	P1A	
13	08 June 2016	P1A	
14	14 June 2016		P1D
15	02 July 2016	P1A	
16	08 July 2016		P1D
17	26 July 2016	P1A	
18	01 August 2016		P1D
19	25 August 2016		P1D
20	31 August 2016	P1A	
21	24 September 2016	P1A	
22	30 September 2016		P1D
23	24 October 2016		P1D
24	30 October 2016	P1A	
25	23 November 2016	P1A	
26	29 November 2016		P1D
27	23 December 2016		P1D
28	29 December 2016	P1A	
29	22 January 2017	P1A	
30	28 January 2017		P1D
31	21 February 2017		P1D
32	27 February 2017	P1A	
33	23 March 2017	P1A	
34	29 March 2017		P1D
35	22 April 2017		P1D
36	28 April 2017	P1A	
37	22 May 2017	P1A	
38	28 May 2017		P1D
39	21 June 2017		P1D
40	27 June 2017	P1A	
41	15 July 2017		P1D
42	21 July 2017	P1A	
43	08 August 2017		P1D
44	20 August 2017		P1D
45	26 August 2017	P1A	

Evaluating the results of both time periods it was proved that the time interval between successive scenes play a significant role in the “number” of pixels located. Small time interval scenes gave back more pixels.

For the image processing as well as for the application of methodology, Gamma Remote Sensing Software (GAMMA Remote Sensing, 2015; Wegmüller *et al.*, 2016a) and SRTM-DEM (Shuttle Radar Topography Mission-Digital Elevation Model) were used. Additionally, in all cases of processing it was chosen: (1) to include all possible interferogram pairs

with 3 scenes, as maximum scene number difference (e.g. 1-2, 1-3, 1-4, 2-3, 2-4, 2-5, etc) and (2) the reference point for image processing to be close to sections under study.

Other important parameters considered and calculated during scene processing, for both time periods and acquisition geometries, can be seen in table 3.

Table 2. List of Sentinel 1A and 1B scenes analysed of Ascending (P2A) and Descending (P2D) acquisition geometry, for the time period extending from January to August 2018

No.	Date	P2A	P2D
1	05 January 2018	P2A	P2D
2	11 January 2018	P2A	P2D
3	17 January 2018	P2A	P2D
4	23 January 2018	P2A	P2D
5	29 January 2018	P2A	P2D
6	04 February 2018	P2A	P2D
7	10 February 2018	P2A	P2D
8	16 February 2018	P2A	P2D
9	22 February 2018	P2A	P2D
10	28 February 2018	P2A	P2D
11	06 March 2018	P2A	P2D
12	12 March 2018	P2A	P2D
13	18 March 2018	P2A	P2D
14	24 March 2018	P2A	P2D
15	30 March 2018	P2A	P2D
16	05 April 2018	P2A	P2D
17	11 April 2018	P2A	P2D
18	17 April 2018	P2A	P2D
19	23 April 2018	P2A	P2D
20	29 April 2018	P2A	P2D

Table 3. Parameters considered and calculated during processing of P1A, P1D, P2A and P2D acquisitions

Master scene used			
P1A	24 th of September 2016		
P1D	24 th of October 2016		
P2A	6 th of March 2018		
P2D	6 th of March 2018		
Average co-registration quality offset responding to azimuth SLC pixel			
P1A	0,0000478		
P1D	0,0001729		
P2A	0,000159		
P2D	-0,0000529474		
	Average Perpendicular Baseline		SLC pairs generated for each section per period
	Asomata	Lefkopetra	
P1A	51,717m	51,884m	57
P1D	52,247m	52,058m	63
P2A	39,105m	39,212	54
P2D	77,651m	77,449	54
cc threshold used for unwrapping the phase of differential interferograms			gamma smoothing parameter
P1A	0,4		0,5
P1D	0,35		0,5
P2A	0,35		0,5
P2D	0,35		0,5

The results obtained are deformation measurements projected along the Line Of Sight (LOS) direction with a rate unit of m/yr. ArcGIS was used to process and map the total velocity of the deformations using as background images provided by Google Earth.

III. ANALYSIS OF MULTITEMPORAL SAR INTERFEROMETRY RESULTS

A lot of methodologies have been suggested in order to calculate the total velocity components of the deformation, from the combination of ascending and descending results, some more complicated than others. Initially in our study two methods were applied, suggested by Manzo *et al.* (2006) and by Notti *et al.* (2014) and Béjar-Pizarro *et al.* (2017). Then, as a third approach, it was chosen to calculate total component by considering results as vectors.

The results of these three methods were compared and were found to be similar, with minor differences. That is why we have chosen to present here only the results of the third approach, which will be described subsequently.

Results, separately for each time period, were analyzed in order to estimate the deformation's total velocity. For each satellite pass, ascending and descending, the results represent deformation rates along the Line Of Sight (LOS) in m/yr (V_A and V_D respectively).

For the analysis we took into consideration that the incidence angle is 34° . Also, in order to calculate the total velocity, only common pixels both in Ascending and Descending geometries were considered. Most importantly, since initial deformation results are obtained in two different viewing geometries (ascending and descending), only a 2 dimensions component can be obtained (East-West and Up-Down-vertical movement). So, in order to proceed, the assumption that the N-S deformation component is insignificant had to be considered and that horizontal movement is analyzed only in an East-West direction component.

On one hand it is obvious that this assumption is imposed by practical limitations. On the other hand, according to Notti *et al.* (2014) for calculating the East-West and Up-Down component for a slope, the slope's direction is not strictly limited to a West (270°) and East (90°) direction, but there is a tolerance of $\pm 45^\circ$ degrees. So, according to Notti *et al.* (2014), the East component is prevalent from 45° (NE) to 135° (SE) and the West component is prevalent from 225° (SW) to 315° (NW). Therefore, for slopes with direction from 45° (NE) to 135° (SE) and from 225° (SW) to 315° (NW) it is "safe" to make the assumption that the contribution of the North-South component is small or insignificant.

The applied procedure can be divided into the following steps:

- For each pass the deformation rates along the LOS were analyzed in vertical and East-West component. Depending whether deformation rates along the LOS are negative or positive, for each pass, the analysis provide positive or negative Vertical and East-West values as presented in table 4 and in figure 2.

Table 4: Analysis of Ascending and Descending deformation rates depending on the sign of initial value

	Ascending	
	Negative values (-)	Positive values (+)
Ascending East-West Component ($V_{EW(A)}$)	Positive value	Negative value
Ascending Vertical Component ($V_{V(A)}$)	Negative value	Positive value

	Descending	
	Negative values (-)	Positive values (+)
Descending East-West Component ($V_{EW(D)}$)	Negative value	Positive value
Descending Vertical Component ($V_{V(D)}$)	Negative value	Positive value

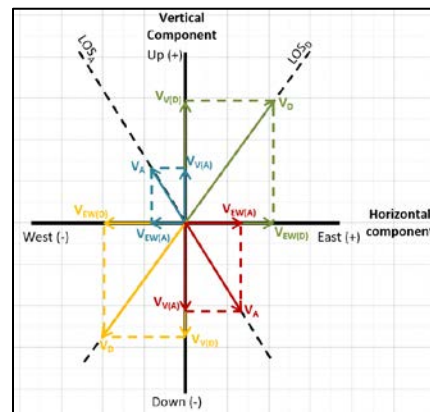


Figure 2. Graphic analysis of positive and negative ascending (V_A) and descending (V_D) deformation rates along the LOS in Vertical (V_V) and East-West (V_{EW}) horizontal components.

- Total vertical (V_V) and East-West (V_{EW}) components were calculated with two ways: a) by summarizing the Ascending and Descending Vertical components and East-West components respectively and b) if Ascending and Descending Vertical components had the same sign for calculating Total Vertical component the average of these two values was calculated and when they had different sign they were summarized. Respectively by the same way the East-West components were calculated.
- Finally, total vertical and East-West components, as calculated with both ways mentioned above, were combined, in order to calculate the total movement component velocity (V_{ol}), for each case, by applying the Pythagorean Theorem. By nature,

the results from the Pythagorean Theorem are positive. For that reason, the sign had to be corrected accordingly, as presented in figure 2 and in table 5.

Additionally, by comparing both Vol from quality point of view, the results were the same, but in the case where Vol was calculated by the combination of Vv and Vew resulting from the first way, a, values were more strengthened and not compatible with to date knowledge regarding deformation phenomena of these areas.

Table 5: Correction of Total movement component (Vol) sign depending on the sign of the Vertical and East-West total component

Total component sign:		Sign of Total movement component (Vol)
Vertical (Vv)	East-West (Vew)	
+	+	+
+	-	+
-	+	-
-	-	-

By this analysis, the results, as vectors, get projected on a vertical plane of an East-West direction.

IV. RESULTS

In this preliminary stage, the results presented hereby is better to be considered as a tool in order to locate areas appearing deformation phenomena and calculated rates not to be considered as absolute values. Also, only the results for the areas or slopes that meet the requirements of direction according to those mentioned above should be considered more reliable. Since, in case of North or South ± 45 degrees direction the South-North component cannot be considered as insignificant.

By taking the above into consideration, aspect maps were produced for the two sections under study and surrounding areas (figure 3a and 3b). While for processing satellite images SRTM-DEM was used, aspect maps were created by the use of a DEM provided by Hellenic Cadastre (Copyright © 2018, Hellenic Cadastre). By definition, when creating an aspect map in ArcMap, classification is as shown in the legend of the maps. However, considering the diagram of figure 3c, where a combination of the classification of the aspect map and of the direction of the slopes is presented in relation to the credibility of estimating only the East-West component, new maps were created. These maps present the domination of the East-West or North-South component (figure 4). Therefore, for Asomata section (figure 4a) in the largest part of the area and clearly around Egnatia Highway, East-West component is prevalent. For Lefkopetra (figure 4b) also in the greater part of the area the East-West component prevails and except some parts, the same is also true for Egnatia. In the

following, some of the results meeting the above requirements selectively are presented in detail.

A. Asomata section

In figures 5a and 5b the results for P1 and P2 time periods are presented respectively. Although the results are not identical, they have similarities and for the common areas in terms of coverage for both time periods, there is no indication for existence of deformation phenomena. For the second time period (P2), where results cover larger areas, two main deforming zones can be identified.

The difference of the results, in terms of the extent of the area covered between P1 and P2 time periods, is because in P2, since time interval between successive scenes is small, coherence is higher.

South of Asomata village, area indicated with A in figure 5b, is a cultivable area and deformation phenomena appearing here can be considered to be related with the existence of a land subsidence zone because of water pumping for farming and animal breeding units (figure 5c). This deformation zone does not affect Egnatia. At the area indicated with B (figure 5b), deformation phenomena appear taking place on an East direction slope of Egnatia Highway (figure 5d). Since at this stage no in situ investigation has taken place, at the moment they cannot be verified.

B. Lefkopetra section

As can be seen in figures 6a and 6b, there is an important difference regarding area coverage between the two time periods, P1 and P2, with almost no results for P1 and extended coverage of our area for P2 period. Additionally, it is observed that P1 results for Lefkopetra section are less informative than these of Asomata for the same period. It is reminded that, for P1, time interval between successive scenes is approximately 30 days. This difference is probably because Lefkopetra area is more mountainous with steeper anaglyph. For P2 where time interval between successive scenes is very short, 6 days, morphology seems to play minor role in affecting the coverage of the area.

For P2 time period, in area noted as A in figure 6b, a zone appearing deformation phenomena can be identified. Their cause is not obvious at this time and in situ investigation has to take place.

Also, locally are detected areas appearing deformation phenomena (e.g. areas noted as B, C, D and E in figure 6b) around Egnatia Highway. In figure 6c is a closer image of area indicated as B and in figure 6d of areas indicated as C and D. Focusing on the area marked as E in figure 6b deformation phenomena appear on both sides crossing the Highway. Their cause is not obvious at this time and in situ investigation has to take place.

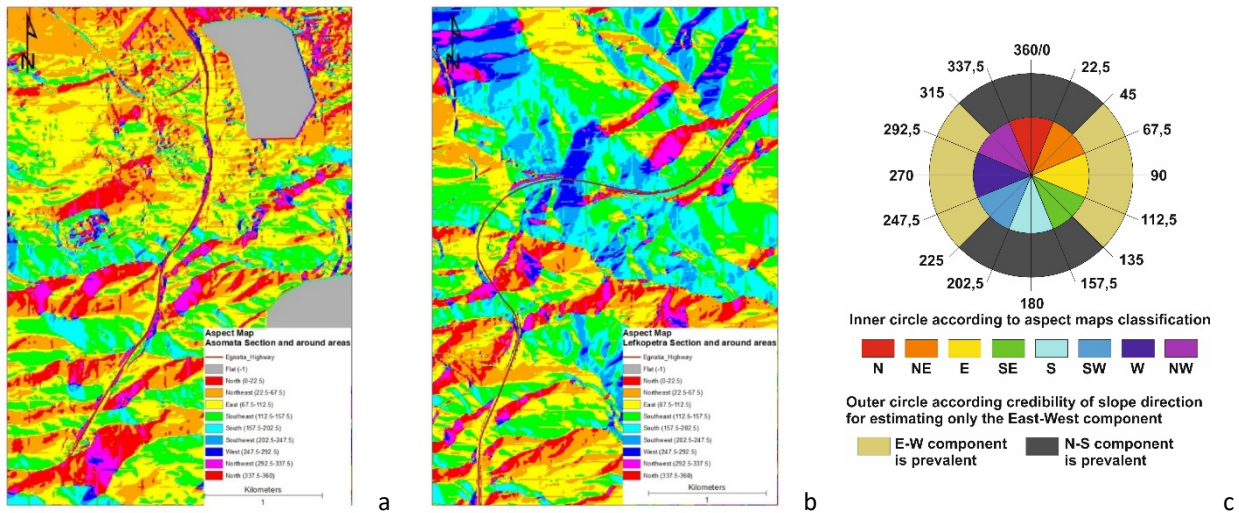


Figure 3. a) and b) Aspect maps of the two sections under study, a) Asomata and b) Lefkopetra and surrounding areas, as emerged from DEM provided from Hellenic Cadastre (Copyright © 2018, Hellenic Cadastre).
 c) Diagram presenting relation between classification of aspect maps of figures 3a and 3b in the inner circle and direction of slopes in relation to credibility of estimating East-West component in the outer circle as seen in maps of figures 4a and 4b.

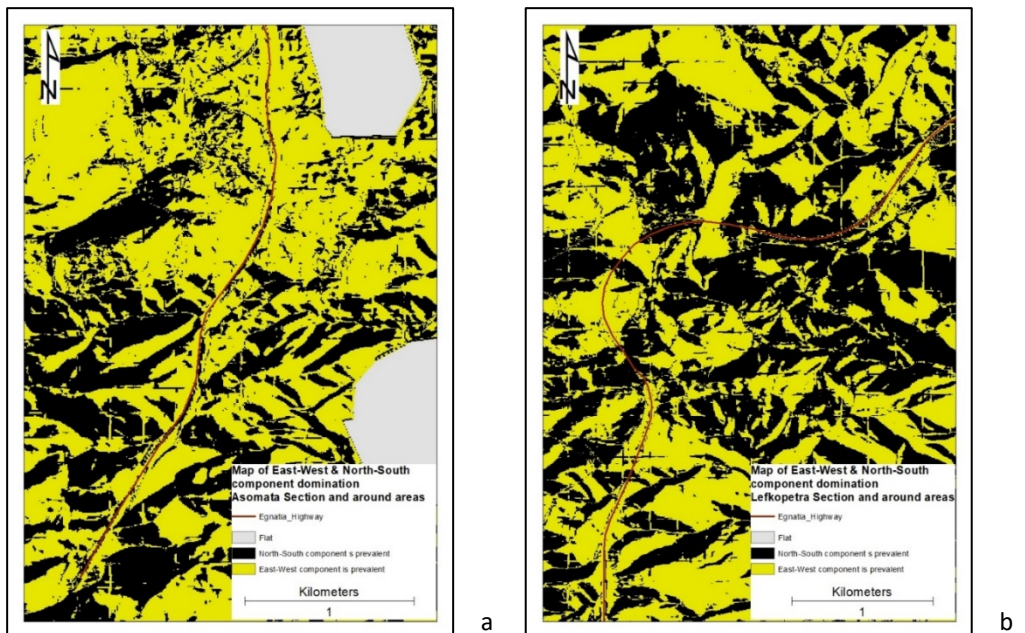


Figure 4. Maps of a) Asomata and b) Lefkopetra and the surrounding areas indicating the domination between East-West and North-South component, as emerged from DEM provided from Hellenic Cadastre (Copyright © 2018, Hellenic Cadastre).

V. CONCLUSIONS

Concluding, total velocity was calculated for slopes and areas surrounding Egnatia Highway with direction 45° - 135° and 225° - 315° , for which East-West component is prevalent. Evaluating the results of the two time periods, it's clear that retrieved deformation results in terms of coverage are better for time period P2, with time interval 6 days, than for P1. Also, comparing the results for P1 between Asomata and Lefkopetra it is obvious that in Lefkopetra, which is more mountainous with steeper relief, results are even more poor for that time period. By that we can conclude that time interval between successive images is critical for the results of the methodology, especially in mountainous areas.

Extensive deformation phenomena along the highway were not detected in any case, for both time periods (P1 and P2). Of course, in situ investigation is needed in order to verify secondary deformations. It should be noted that the deformation results can be used only to identify areas presenting deformation and they cannot be evaluated for their absolute deformation rates.

As these are preliminary results of research carried out in these sections of Egnatia Highway, except of in situ investigation, the intention is to compare them with instrumental measurements from the areas. Following that, research will be extended in other sections of the Highway for longer time periods with time interval of 6 days between successive images.

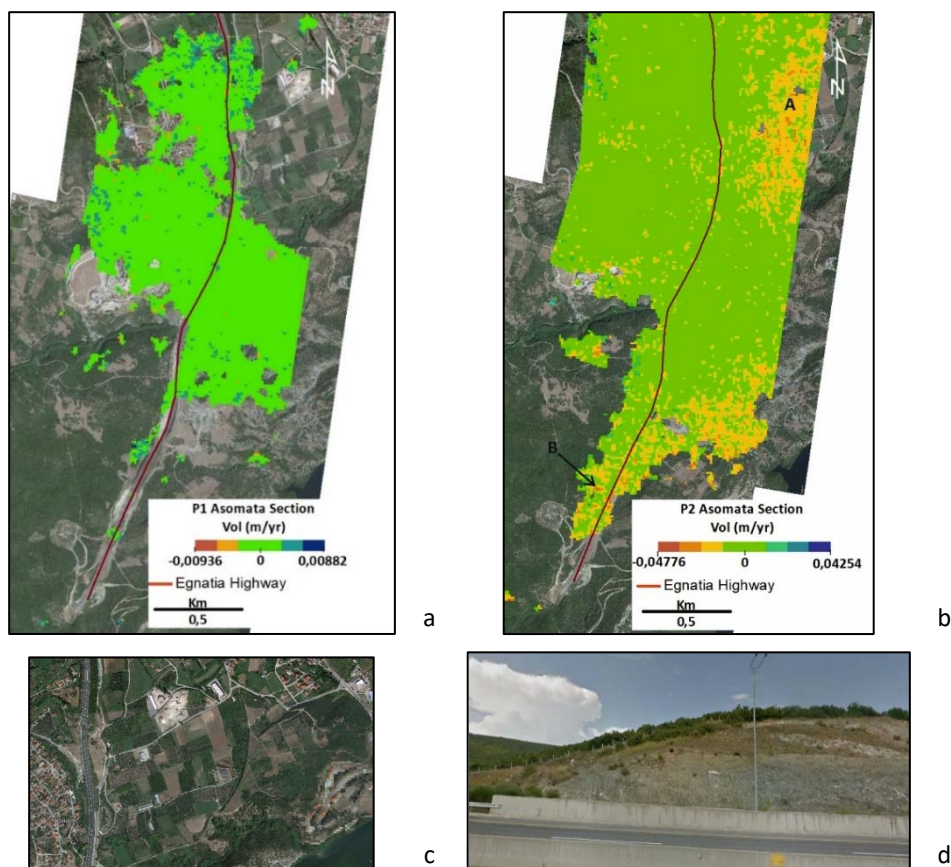


Figure 5. Total component of deformation rates in m/yr for time periods P1 (a) and P2 (b) for Asomata section. In c) and d) are detailed views of the areas indicated with A and B respectively, presenting deformation phenomena.

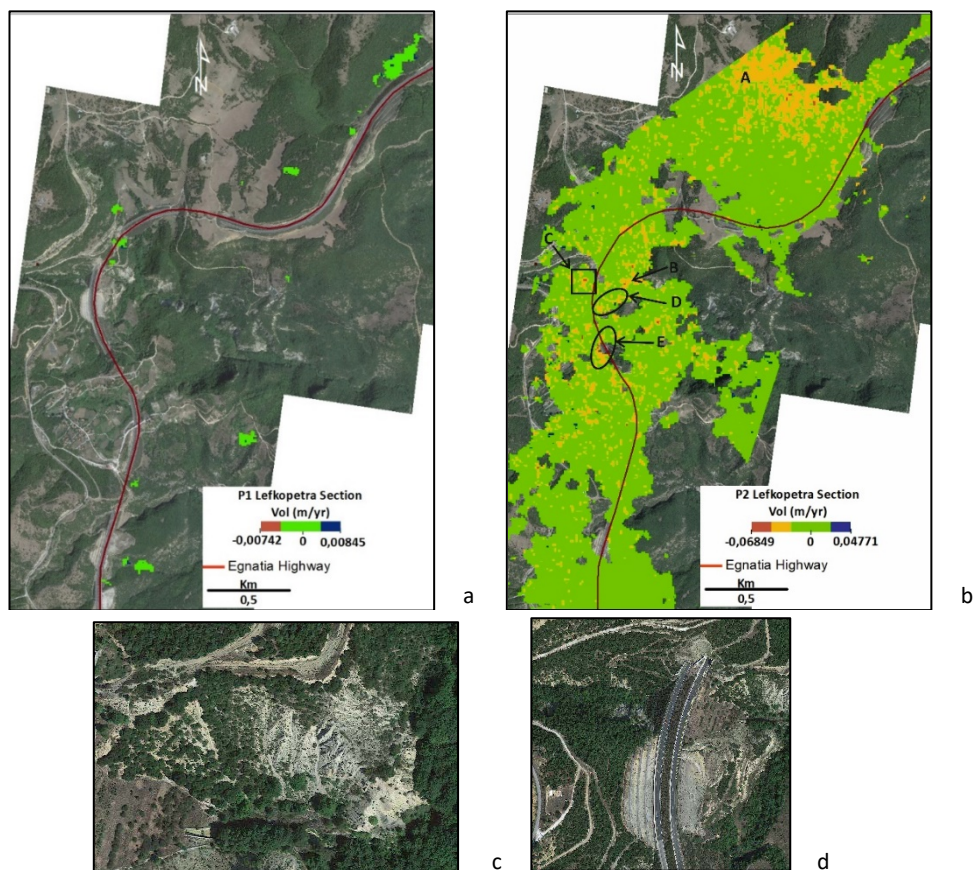


Figure 6. Total component of deformation rates in m/yr for time periods P1 (a) and P2 (b) for Lefkopetra section. In figures c) and d) are detailed images of areas indicated with B and C-D respectively, where deformation phenomena occur.

References

- Barra, A., O. Monserrat, P. Mazzanti, C. Esposito, M. Crosetto, G.Sc. Mugnozza (2016). First insights on the potential of Sentinel-1 for landslide detection. *Geomatics, Natural Hazards and Risk*, Vol. 7, Issue 6, pp. 1874-1883.
- Béjar-Pizarro, M., D. Notti, R.M. Mateos, P. Ezquerro, G. Centolanza, G. Herrera, G. Bru, M. Sanabria, L. Solari, J. Duro, J. Fernández (2017). Mapping Vulnerable Urban Areas Affected by Slow-Moving Landslides Using Sentinel-1 InSAR Data. *Remote Sensing*, Vol 9, Issue 9, No 876.
- Bellotti, F., M. Bianchi, D. Colombo, A. Ferretti, A. Tamburini (2014). Advanced InSAR Techniques to support landslide monitoring. *Mathematics of Planet Earth, Lecture Notes in Earth System Sciences*, E. Pardo-Igúzquiza et al. (eds.), Springer-Verlag Berlin (publ.), pp. 287-290.
- Berardino, P., G. Fornaro, Lanari R., Sansosti E. (2002). A new algorithm for surface deformation monitoring based on small baseline differential SAR interferograms. *IEEE Transactions on Geoscience and Remote Sensing*, Vol 40, Issue 11, pp. 2375-2383.
- Bernardi, G., F. Procopio (2013). Intergrating landslide monitoring into Multi-Hazard Monitoring Systems. In *Landslide Science and Practice*, C. Margottini et al. (eds), Springer-Verlag Berlin (publ.), Vol. 2, pp. 559-565.
- Cardellini St., P. Osimani (2013). The Ancona early warning centre, instrumentation and continuous monitoring of the landslides. In *Landslide Science and Practice: Early Warning, Instrumentation and Monitoring*, Margottini, Canuti & Sassa (eds), Springer (publ.), Vol. 2, pp. 57-65.
- Copernicus Sentinel Data (2016-2018), processed by ESA.
- Dong, J., L. Zhang, M. Li, Y. Yu, M. Liao, J. Gong, H. Luo (2018). Measuring precursory movements of recent Xinmo landslide in Mao County China with Sentinel1 and ALOS-2 PALSAR-2 datasets. *Landslides*, Vol. 15, pp. 135-144.
- Ferretti, A., C. Prati, F. Rocca (2000). Nonlinear subsidence rate estimation using permanent scatterers in differential SAR interferometry. *IEEE Transactions on Geoscience and Remote Sensing*, Vol 38, Issue 5, pp. 2202-2212.
- Ferretti, A., C. Prati, F. Rocca (2001). Permanent Scatterers in SAR Interferometry. *IEEE Transactions on Geoscience and Remote Sensing*, Vol 39, Issue 1, pp. 8-20.
- Frodella, W., A. Ciampalini, F. Bardi, T. Salvatici, F. Di Traglia, G. Basile, N. Casagli (2018). A method for assessing and managing landslide residual hazard in urban areas. *Landslides*, Vol. 15, Issue 2, pp. 183-197.
- GAMMA Remote Sensing (2015). Sentinel-1 processing with GAMMA software: Documentation-user's guide. *GAMMA Remote Sensing*, version 1.2, Dec2015, 39p.
- Gaprindashvili, G., C.J. Van Westen (2016). Generation of a national landslide hazard and risk map for the country of Georgia. *Natural Hazards*, Vol. 80, pp. 69-101.
- Manzo, M., G.P. Ricciardi, F. Casu, G. Ventura, G. Zeni, S. Borgström, P. Berardino, C. Del Gaudio, R. Lanari (2006). Surface deformation analysis in the Ischia Island (Italy) based on spaceborne radar interferometry. *J. of Volcanology Geothermal Research*, Vol. 151, Issue 4, pp. 399-416.
- Mazzanti, P., Fr. Bozzano, A. Brunetti, P. Caporossi, C. Esposito, G.Sc. Mugnozza (2017). Experimental landslide monitoring site of Poggio Baldi Landslide (Santa Sofia, N-Apennine, Italy). *Advancing Culture of Living with Landslides, 4th WLF, Ljubljana, Slovenia, 2017*, M. Mikoš et al. (publ.), Springer International (publ.), pp. 259-266.
- Notti, D., G. Herrera, S. Bianchini, Cl. Meisina, J.C. García-Davallillo, Fr. Zucca (2014). A methodology for improving landslide PSI data analysis. *Int. J. of Remote Sensing*, Vol. 35, No. 6, pp. 2186-2214.
- Notti, D., J.P. Galve, R.M. Mateos, O. Monserrat, Fr. Lamas-Fernández, Fr. Fernández-Chacón, Fr.J. Roldán-García, J.V. P'erez-Pena, M. Crosetto, J.M. Azanón (2015b). Human-induced coastal landslide reactivation. Monitoring by PSInSAR techniques and urban damage survey (SE Spain). *Landslides*, Vol. 12, pp. 1007-1014.
- Notti, D., Cl. Meisina, Fr. Zucca, Al. Colombo, L. Paro (2015a). Map and monitoring slow ground deformation in NW Italy using PSI Techniques. *Engineering Geology for Society and Territory*, G. Lollino et al. (eds), Vol. 5, pp. 141-145.
- Pecoraro, G., M. Calvello, L. Piciullo (2019). Monitoring strategies for local landslide early warning systems. *Landslides*, Vol. 16, Issue 2, pp. 213-231.
- Plank, S., M. Krautblatter, K. Thuro (2015). Feasibility assessment of landslide monitoring by means of SAR Interferometry: A case study in the Ötztal Alps, Austria. *Engineering Geology for Society and Territory*, G. Lollino et al. (eds), Vol. 2, pp. 375-378.
- Refice, A., L. Spalluto, F. Bovenga, A. Fiore, M.N. Miccoli, P. Muzzicato, D.O. Nitti, R. Nutricato, G. Pasquariello (2019). Intergration of persistent scatterer interferometry and ground data for landslide monitoring: the Pianello landslide (Bovino, Southern Italy). *Landslides*, Vol. 16, Issue 3, pp. 447-468.
- Roberts, N.J., B. Rabus, R.L. Hermanns, M.-A. Guzmán, J.J. Clague, E. Minaya (2014). Recent landslide activity in La Paz, Bolivia. *Landslide Science for a Safer Geoenvironment*, Sassa et al. (eds.), Springer Int. (publ.), Vol. 3, pp. 431-437.
- Tessari, G., M. Floris, Vl. Achilli, M. Fabris, A. Menin, M. Monego (2017). Testing Sentinel-1A Data in Landslide Monitoring: a case study from North-Eastern Italian Pre-Alps. *Advancing Culture of Living with Landslides, 4th WLF, Ljubljana, Slovenia, 2017*, M. Mikoš et al. (publ.), Springer Int. (publ.), pp. 209-217.
- Yao, G., C.-Q. Ke, J. Zhang, Y. Lu, J. Zhao, H. Lee (2019). Surface deformation monitoring of Shanghai based on ENVISAT ASAR and Sentinel-1A data. *Env. Earth Sciences*, Vol. 78, doi.org/10.1007/s12665-019-8226-z, in print.
- Wegmüller, U., Ch. Werner, T. Strozzi, A. Wiesmann, O. Frey, M. Santoro (2016a). Sentinel-1 Support in the GAMMA Software. *Procedia Computer Science*, Vol. 100, pp. 1305-1312.
- Wegmüller, U., Ch. Werner, A. Wiesmann, T. Strozzi, P. Kourkoulis, O. Frey (2016b). Time-series analysis of Sentinel-1 Interferometric Wide Swath data: techniques and challenges. *Proceedings IEEE International Geoscience and Remote Sensing Symposium*, Beijing, China, WE4-L10.3, pp. 3898-3901.
- Werner, C., U. Wegmüller (2008). ALOS PALSAR quality assessment, calibration and validation research. *ALOS Research and Application Project of EORC, JAXA*, PI Number 175, 3p.
- Werner, C., U. Wegmüller, Strozzi T., Wiesmann A. (2003). Interferometric Point Target Analysis for deformation mapping. *Proceeding IEEE Int. Geoscience and Remote Sensing Symp.*, Toulouse, France, Vol. 7, pp. 4362-4364.